DENTAL MATERIALS 39 (2023) 320–332

Available online at www.sciencedirect.com

ScienceDirect

journal homepage: www.elsevier.com/locate/dental

Morphology and mechanical performance of dental crown designed by 3D-DCGAN

Hao Ding [a], Zhiming Cui [b,c], Ebrahim Maghami [d], Yanning Chen [a], Jukka Pekka Matinlinna [a,e], Edmond Ho Nang Pow [f], Alex Siu Lun Fok [g], Michael Francis Burrow [f], Wenping Wang [b,h], James Kit Hon Tsoi [a,*]

[a] Dental Materials Science, Applied Oral Sciences and Community Dental Care, Faculty of Dentistry, The University of Hong Kong, Hong Kong
[b] Department of Computer Science, Faculty of Engineering, The University of Hong Kong, Hong Kong
[c] School of Biomedical Engineering, ShanghaiTech University, Shanghai, China
[d] Department of Mechanical Engineering and Mechanics, College of Engineering, Drexel University, Philadelphia, USA
[e] Division of Dentistry, School of Medical Sciences, The University of Manchester, Manchester, UK
[f] Restorative Dental Sciences, Faculty of Dentistry, The University of Hong Kong, Hong Kong
[g] Minnesota Dental Research Center for Biomaterials and Biomechanics, School of Dentistry, University of Minnesota, USA
[h] Department of Visualization, College of Architecture, Texas A&M University, USA

ARTICLE INFO

Article history:
Received 3 May 2022
Received in revised form 6 February 2023
Accepted 14 February 2023

Keywords:
3D-DCGAN
Artificial Intelligence
Dental Crown
Design
CAD/CAM

ABSTRACT

Objectives: This study utilised an Artificial Intelligence (AI) method, namely 3D-Deep Convolutional Generative Adversarial Network (3D-DCGAN), which is one of the true 3D machine learning methods, as an automatic algorithm to design a dental crown.

Methods: Six hundred sets of digital casts containing mandibular second premolars and their adjacent and antagonist teeth obtained from healthy personnel were machine-learned using 3D-DCGAN. Additional 12 sets of data were used as the test dataset, whereas the natural second premolars in the test dataset were compared with the designs in (1) 3D-DCGAN, (2) CEREC Biogeneric, and (3) CAD for morphological parameters of 3D similarity, cusp angle, occlusal contact point number and area, and *in silico* fatigue simulations with finite element (FE) using lithium disilicate material.

Results: The 3D-DCGAN design and natural teeth had the lowest discrepancy in morphology compared with the other groups (root mean square value = 0.3611). The Biogeneric design showed a significantly ($p < 0.05$) higher cusp angle (67.11°) than that of the 3D-DCGAN design (49.43°) and natural tooth (54.05°). No significant difference was observed in the number and area of occlusal contact points among the four groups. FE analysis showed that the 3D-DCGAN design had the best match to the natural tooth regarding the stress distribution in the crown. The 3D-DCGAN design was subjected to 26.73 MPa and the

* Correspondence to: Dental Materials Science, Applied Oral Sciences and Community Dental Care, Faculty of Dentistry, The University of Hong Kong, 1B18, Prince Philip Dental Hospital, 34 Hospital Road, Hong Kong.
E-mail address: jkhtsoi@hku.hk (J.K.H. Tsoi).

https://doi.org/10.1016/j.dental.2023.02.001

natural tooth was subjected to 23.97 MPa stress at the central fossa area under physiological occlusal force (300 N); the two groups showed similar fatigue lifetimes (F-N curve) under simulated cyclic loading of 100–400 N. Designs with Biogeneric or technician would yield respectively higher or lower fatigue lifetime than natural teeth.

Significance: This study demonstrated that 3D-DCGAN could be utilised to design personalised dental crowns with high accuracy that can mimic both the morphology and biomechanics of natural teeth.

1. Introduction

With current advances in technology, digitisation has evolved in various industries. In dentistry, computer-aided design and computer-aided manufacturing (CAD/CAM) have created great opportunities to improve the productivity of dental prostheses. The conventional workflow for preparing dental prostheses is labour-intensive and time-consuming, generating health and environmental hazards. Although improved, the current CAD/CAM technology still encounters such problems. Each dental prosthesis must be customised to meet individual patient conditions and requirements. Even with the assistance of CAD software, this is a time-consuming and labour-intensive process.

Artificial Intelligence (AI) is the science and engineering of machines that act intelligently [1]. One of the pioneers of AI in crown design is CEREC Software; the algorithm [2,3] tries to find the mathematical relationships between the existing tooth morphology, tooth preparation, and adjacent and opposite teeth. Hence, it can fit customised conditions for individual patients. However, remaking CAD/CAM crowns is not uncommon clinically because of marginal misfits [4]. The crown design also impacts the fracture behaviour of crowns and thus influences clinical outcomes [5]. Deep learning (DL) is a branch of AI, and in dentistry, most applications involve automatic diagnosis based on optical or radiology images [6,7]. Introduced by Goodfellow et al. [8], the generative adversarial network (GAN) is an algorithm based on DL to analyse the training data distribution to generate new data following the same distribution. Hwang et al. [9] applied a GAN model to generate a crown, particularly in dental crown design. However, the study used a two-dimensional (2D) depth-projection method to learn data from dental prostheses designed by a dental laboratory. Some morphological features may be compromised during the 2D to 3D transformation. Furthermore, using dental laboratory prostheses as training data (ground truth) for DL is also questionable because the dentist usually adjusts a prosthesis at the chairside after receiving it from the dental laboratory; thus, the GAN model learns inaccurate morphology information. Recently, Yuan et al. [10] proposed an automatic occlusal surface design method based on conditional GAN and achieved satisfactory results. However, it is a 2D pix2pix method that cannot fully reflect the 3D requirements of a tooth. A deep convolutional GAN (DCGAN) is a type of GAN introduced by Radford et al. [11], specifically for unsupervised learning. In 2016, Wu et al. [12] introduced a 3D shape generative model, 3D-DCGAN, which can be regarded as a natural extension of DCGAN in 3D space, extending its application to 3D images.

An essential factor in the design of dental prostheses is occlusal surface design. The grooves and cusps follow a specific shape to assist the mastication and stability of the lower jaw. There are different recommendations and guidelines regarding the design, such as cusp angle, cuspal inclination, position and depth of grooves, ridges, bevels, and chamfers. These represent the current cognition of biological and mechanical ideas that are eventually perceived as functional and aesthetic requirements [13,14].

The long-term effectiveness of all-ceramic crowns is essential yet challenging to evaluate. It is not only affected by the material used but also by the crown design. Finite element analysis (FEA) is instrumental in studying different designs that may not be clinically achievable. For example, Maghami et al. [15] studied different crown designs using FEA and found that crown height plays a more significant role because increasing the bonding area can relieve stress. More recently, a non-linear 3D FEA has been developed that can predict the fatigue lifetime of dental crowns on human teeth with a good match with the experimental results [16]. Thus, FEA is a useful biomechanical evaluation tool that can provide helpful information to dental researchers and clinicians regarding different materials and design combinations.

This study aimed to develop a true 3D AI algorithm for dental crown design. This will provide a functional AI tool used in dentistry that can innovate and automate the current digital dental prosthetic workflow.

2. Materials and methods

2.1. Dataset

Six hundred digital casts with full arches of both the upper and lower jaws and occlusal relationships were obtained with informed consent (IRB Reference Number: UW 21–571) from healthy personnel (average age of 20.84 years old) using an intraoral scanner (Cerec Omnicam, Sirona Dental Systems, Bensheim, Germany). Standard Tessellation Language (STL) files were exported from CEREC Software 4.6 (Sirona Dental Systems, Bensheim, Germany). In this study, tooth numbers 44, 45, and 46 (Fig. 1A) in the ISO 3950 notation system were segmented manually using Meshlab software (ISTI-CNR, Pisa, Italy) [17], where 45 was the target, and 44 and 46 (Fig. 1B) were used as a reference for 3D-DCGAN model training.

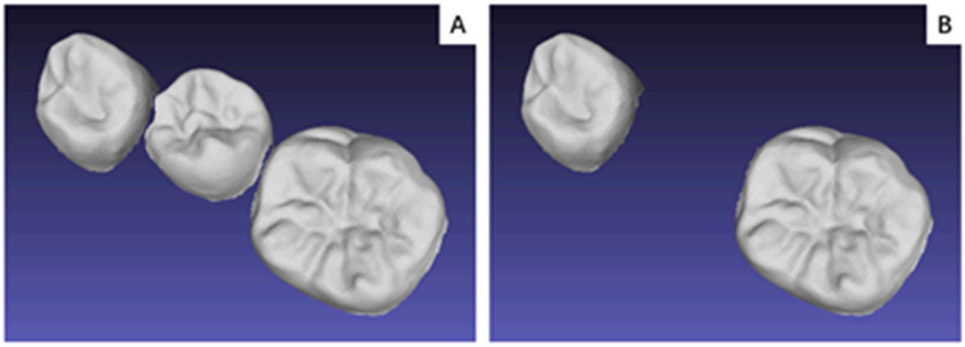

Fig. 1 – One set of training data A) No. 44, 45, 46 tooth; B) No. 44, 46 tooth.

2.2. *GAN Training*

A 3D-DCGAN was adopted to train the machine learning model. The network was built on the PyTorch platform. The generator model consisted of four deconvolution layers with the number of filters as 128–64–32–1. The kernel size, stride, and padding size were set to $3 \times 3 \times 3$, 1, and 1, respectively. A Tanh function was used in the last layer of the generator. The discriminator model consisted of four convolution layers, reflecting the same structure as the generator. With the exception that the stride was set to two, a sigmoid function was applied at the last layer of the discriminator. Batch normalisation was performed after each convolutional layer. LeakyReLUs were used in the generator and discriminator models, with a slope of 0.2.

The training was performed on a desktop computer with an Intel(R) Xeon (R) W-2123 3.6 GHz CPU, an Nvidia GeForce RTX 2080 Ti GPU, and 16 GB RAM. Different parameters, such as learning rate, batch size, number of epochs, and training data, were investigated to determine the optimal parameters. To monitor the quality of the generated tooth morphology with increasing epochs, the interval between image sampling was set to 400, *i.e.* the training results were exported and saved every 400 epochs.

2.3. *Quality evaluation*

Twelve additional cases were randomly selected as the testing dataset, and 12 crowns were generated using the trained 3D-DCGAN. These AI crowns were compared with the original natural tooth (NT), CEREC biogeneric individual design (BI), and technician CAD (Zfx Manager 2.0, Zfx GmbH, Dachau, Germany) design (TD) operated by an experienced dental technician with respect to the cusp angle, 3D similarity, occlusal contact, and dynamic FEA.

2.3.1. *Cusp angle*

Cusp angle (Fig. 2) is an important parameter in the dental crown design process. This affects the fracture resistance of the crowns. In general, a wider cusp angle can enhance the fracture resistance of the crown [18]. The cusp angles in all four groups (NT, AI, BI, and TD) were measured and compared. The crown designs were cut cross-sectionally, and the cusp angles were measured using Geomagic Control 2014 software (3D Systems, Rock Hill, SC, USA).

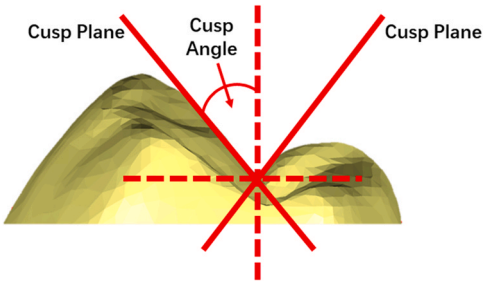

Fig. 2 – A vertical cross-sectional view of a premolar indicating cusp angle and cusp plane.

2.3.2. *3D Comparison*

The degree of discrepancy between the NT group and the other design groups was compared using the Geomagic software. With the NT group set as a reference, crowns from the other three groups (AI, BI, and TD) were superimposed with the reference crown using a best-fit algorithm and pairwise compared with the crown in the NT group. Irrelevant areas were cut, and only occlusal surfaces were reserved to eliminate errors during the comparison. The 3D measurement function was used to compare and calculate the discrepancies between different comparisons. The deviation analysis function was used to evaluate the degree of discrepancy, and the mean positive/negative deviation and Root Mean Square (RMS) values were recorded.

2.3.3. *Occlusal contact measurement*

A digital approach was adopted to measure the occlusal contact point number and area using the Geomagic software. The STL file of the tooth to be measured and its opposing dentition was imported into the software. A virtual articulating paper approach was adopted by moving the teeth 100 µm and 200 µm perpendicular to the occlusal surface. The 100 µm and 200 µm offset represented the thicknesses of the articulating paper. Boolean operations were then performed to maintain the upper and lower dentition intersecting parts.

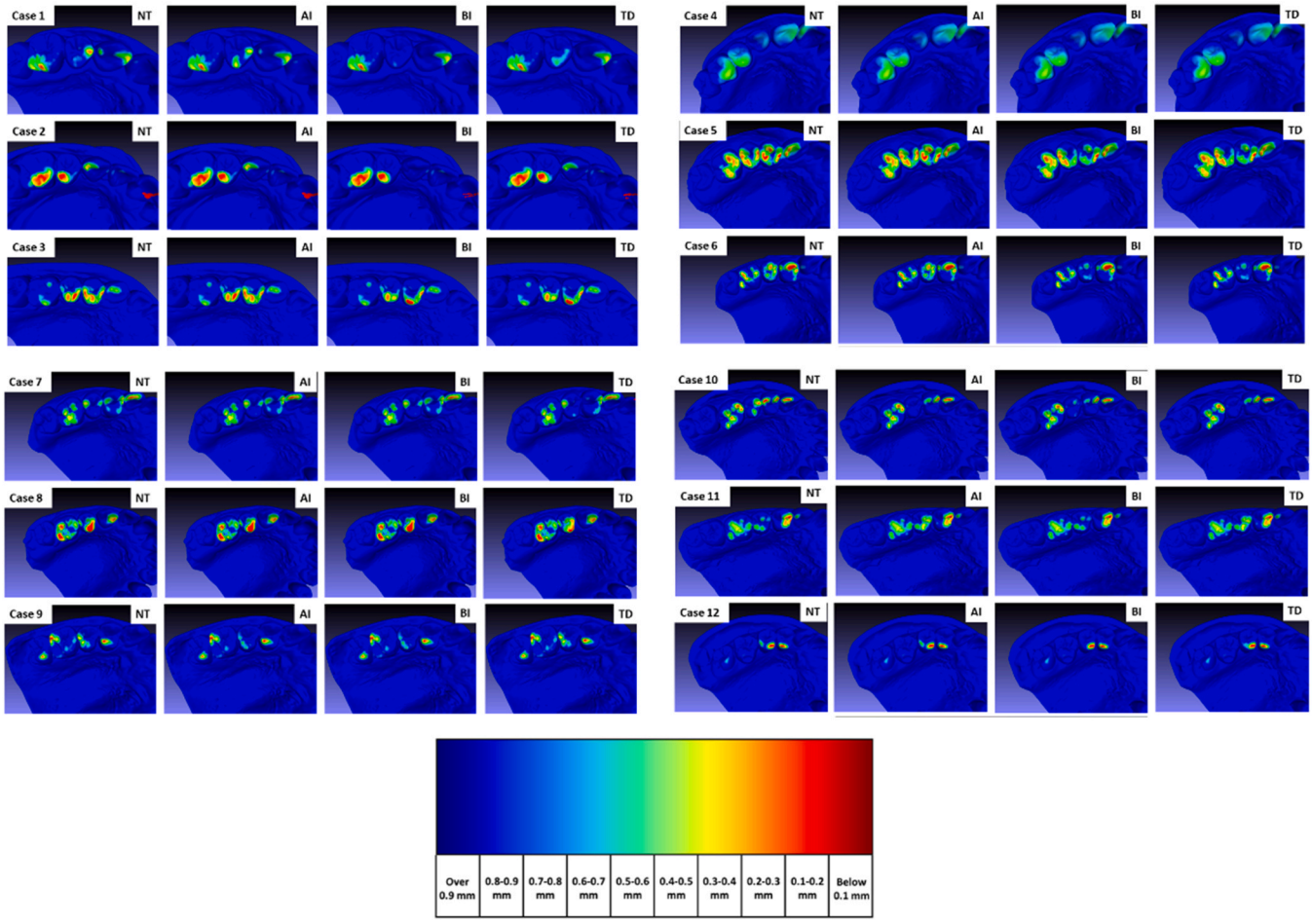

Fig. 3 – Occlusal contact number and area of the NT, AI, BI and TD groups, cases 1–12.

The occlusal contact point number and area on the opposing dentition were then calculated accordingly.

To better simulate tooth movement, four horizontal excursive positions from maximal intercuspation were simulated: 0.5, 1.0, 2.0, and 3.0 mm. The excursive process was performed by horizontally displacing the opponent dentition away from the crown model and adjacent teeth, which simulates the occlusal in actual conditions.

After fixing the horizontal displacement, vertical adjustment was conducted to fit the occlusal relationship between the maxillary and mandibular casts. The crown and its adjacent teeth to be tested were vertically shifted away from the opposing dentition in a 0.05 mm increment. Once the contact between the testing and the opposing dentition disappeared, the testing sample was shifted vertically towards the opposing dentition by 0.05 mm. This process enabled the examination of the working side contacts of the teeth in the occlusion relationship [19]. The models in all four groups followed the same protocol described above to ensure consistency. The steepness was calculated by relating the vertical mandibular offset to the horizontal displacement to quantify the level of vertical movement. The following equation was used to calculate the angle of steepness in degrees.

$$\theta = \tan^{-1}\frac{HorizontalDisplacement}{VerticalOffset} \quad (1)$$

where θ represents the angle of steepness. A higher θ value indicates higher occlusal steepness [20].

The MeshLab software was used to visualise the occlusal relationship. A distance heat map can be obtained at the opposite dentition using the functions “Distance from Reference Mesh” and “Colorize by Vertex Quality”. A 0–1 mm range of occlusal distance was selected. Given that the thickness of bite registration for dental use ranges from 8 to 200 µm, we included the distance below 200 µm as the contact area (red area in the heat map shown in Fig. 3). The number of contact points and areas can be obtained by the software accordingly (“Select by Vertex Quality” function followed by “Compute Area” function). The contact point numbers and areas obtained from Meshlab were compared with those obtained from Geomagic to verify the agreement between the two software packages.

2.3.4. *Dynamic Finite Element Analysis*

One mandibular second premolar with the same tooth preparation and four crown designs (NT, AI, BI, and TD) was selected randomly from the test group. A 50 µm adhesive layer was created by an offset function in Abaqus software (version

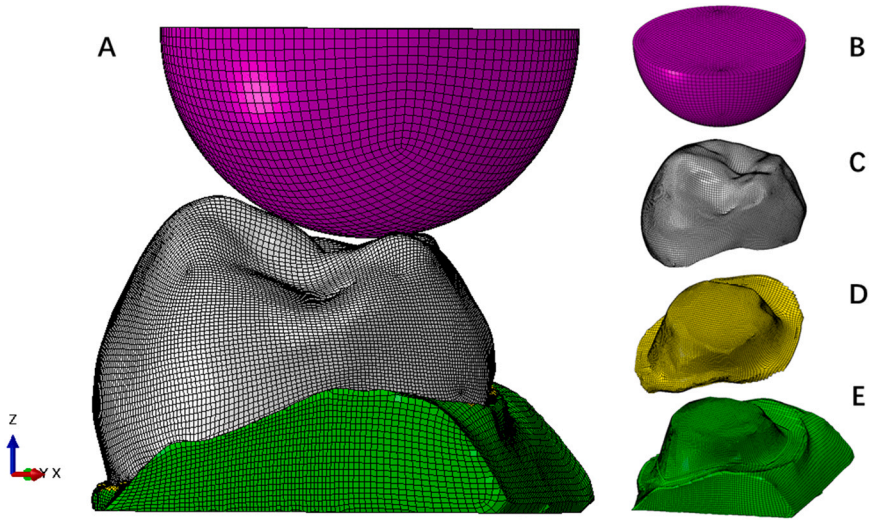

Fig. 4 – Schematics showing the structure of FE model: A) testing position of the whole model; B) indenter; C) ceramic crown; D) adhesive layer and E) dentine.

6.5, ABAQUS Inc., Providence, RI, USA). Subsequently, a validated dynamic non-linear finite element (FE) model [16] was used to evaluate the biomechanical fatigue performance of lithium disilicate on human teeth *in silico*. In brief, a multi-block technique was adopted to simulate the complex details of the tooth surface, and hexahedral meshes were created [21]. The imported STL files are processed by assigning blocks to the current STL mesh. The volumetric hexahedral mesh of the crown, adhesive layer, and abutment tooth was created using the IA-FEMesh software (University of Iowa, Iowa City, IA, USA).

As illustrated in Fig. 4, the final model for FEA consists of a crown, adhesive layer, and abutment tooth. A stainless steel hemisphere with a diameter of 5 mm was created as the indenter. The hemisphere indenter was positioned precisely above the occlusal surface using SolidWorks (Dassault Systémes SolidWorks Corp., Waltham, MA, USA). The indenter was then fine-tuned and settled frictionlessly near the central fossa area, with two contact points on the buccal and lingual cusps contacting the indenter simultaneously.

All models with their position information were then transferred to the Abaqus software. Lithium disilicate (LD) was selected as the crown material, and dentin was selected as the abutment material in the FE simulation. The required mechanical properties of the different materials used in the FEA model, such as Young's modulus and Poisson's ratio for the crown materials, adhesive cement, and dentine, were obtained from the literature [22–25] and are shown in Table 1. All parts of the model were assumed homogeneous, isotropic, and linearly elastic.

The fatigue life of the LD ceramic crowns was calculated by comparing the maximum principal stress reached during loading with their stress-life (S-N) diagrams. The non-linear Basquin formula (Eq. 2) [26,27] was used to fit the fatigue behaviour of the crown material.

$$\sigma_a = A(N)^B \quad (2)$$

where σ_a is the stress amplitude, N is the fatigue life circles, and A and B are two material constants obtained from previous literature [28,29] and are listed in Table 1. Then, occlusal forces from 100 to 400 N were applied to compare the stress distributions in different crown designs. Occlusal forces were selected based on natural occlusal forces for human premolars [30].

2.4. *Statistical analysis*

Statistical analysis was performed using SPSS software (version 27.0; IBM, Armonk, NY, USA). The statistical significance of the cusp angle, 3D discrepancy, and occlusal contact among the four design groups was studied using one-way analysis of variance (ANOVA) and Tukey's HSD *post hoc* multiple comparisons. The level of significance was set at $\alpha = 0.05$.

3. Results

3.1. *Cusp angle*

Table 2 shows the cusp angles for the different crown designs. The mean cusp angles of the NT, AI, BI, and TD groups

Table 1 – Mechanical parameters, coefficient and exponent constants of fatigue curves of LD ceramic, dentine and adhesive resin cement.

Materials	Young's Modulus (GPa)	Poisson's Ration	A (MPa)	B
LD Ceramic	95.9	0.23	95.845	-0.012
Dentine	18.6	0.31		
Adhesive Resin Cement	7.7	0.3		

Table 2 – Mean cusp angle of the four crown designs.

Groups	Mean (SD) (Unit: degree)	SE
NT	54.05 (5.11)[a]	1.47
AI	49.43 (5.53)[a]	1.60
BI	67.11 (4.53)[b]	1.31
TD	63.34 (4.98)[ab]	1.44

*Different superscript letters indicate significant differences ($p < 0.05$)

were respectively 54.05°, 49.43°, 67.11° and 63.34°. The NT group had a significantly lower mean cusp angle than the BI group, whereas the BI and TD groups had significantly higher mean cusp angles than the AI group. No significant differences were found between the NT, AI, NT, and TD groups.

3.2. 3D Morphology comparison

The discrepancy of crown designs in the AI, BI, and TD groups was compared pairwise with the NT group. A heat map of the discrepancy between the NT and AI groups is shown in Fig. 5. The colour transitioned from blue to red, representing the contraction to the expansion of the crown surface from −1.5 to 1.5 mm. The results of the numerical comparison are presented in Table 3.

As indicated in Table 3, the NT vs. AI group exhibited the lowest statistically significant discrepancy in mean positive deviation (MPD), mean negative deviation (MND), and root mean square (RMS) values. The discrepancy between the NT vs. BI group and the NT vs. TD group was not statistically significant for the last two items (MND and RMS). In addition, the NT vs. BI group exhibited significantly lower MPD values than those of the TD vs. NT group.

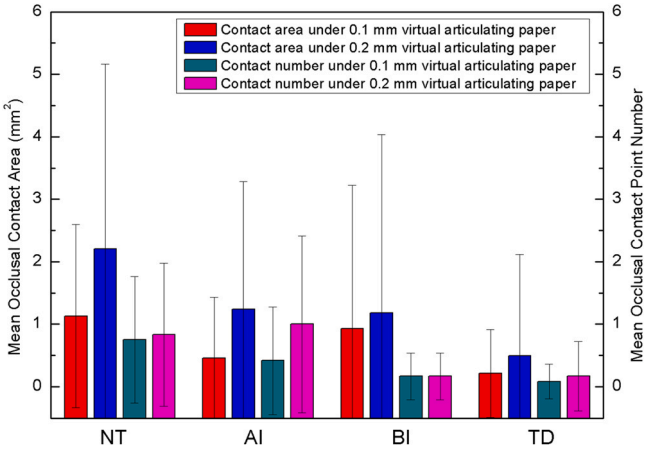

Fig. 6 – Mean occlusal contact point number and area of the crowns in different groups.

3.3. Occlusal Contact

Two types of virtual articulating papers with thicknesses of 100 µm and 200 µm were used. The occlusal contact point number and area were measured for all groups. Fig. 6 shows the mean contact point number and area for the NT, AI, BI, and TD groups. The contact point numbers and areas for 100 µm and 200 µm articulating papers did not differ significantly between the four groups.

A horizontal displacement was applied to simulate the transverse working plane. As illustrated in Fig. 7, gradual decreases in the contact point number were observed for the NT, AI, and TD groups, except for group BI, which tended to increase with the 100 µm virtual articulating paper. The TD

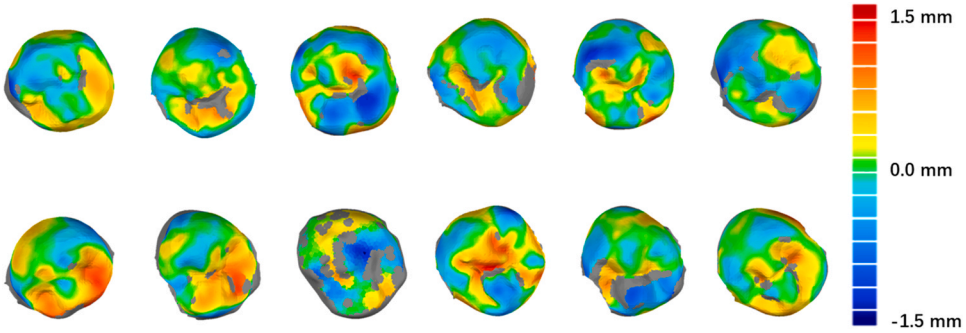

Fig. 5 – Heat map of the discrepancy of the AI and NT groups.

Table 3 – Comparison of the mean discrepancy of crowns in the AI, BI and TD groups with the NT group.

Groups	Mean Positive Deviation (SD)	Mean Negative Deviation (SD)	Root Mean Square (SD)
NT vs. AI	0.2502 (0.0494)[a]	-0.3106 (0.1215)[d]	0.3611 (0.1160)[f]
NT vs. BI	0.3480 (0.0576)[b]	-0.4379 (00883)[e]	0.5065 (0.0700)[g]
NT vs. TD	0.2919 (0.0455)[c]	-0.3894 (0.1183)[e]	0.4550 (0.1019)[g]

*Different superscript letters indicate significant differences ($p < 0.05$)

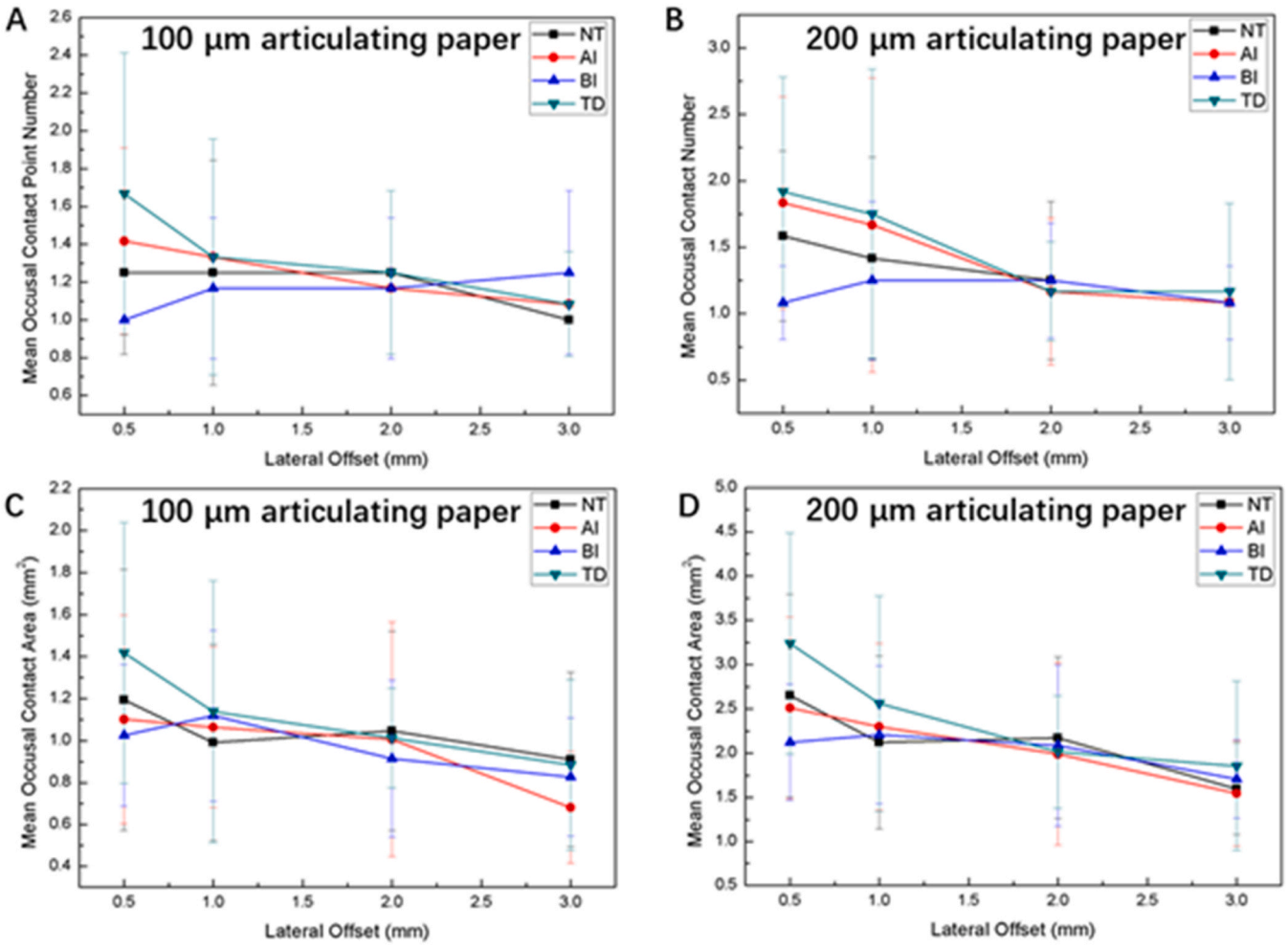

Fig. 7 – Trend of mean occlusal contact point number (A and B) and area (C and D) when increasing the offset from 0.5 to 3.0 mm on the lateral occlusion using different virtual articulating paper.

group had a more prominent decrease in the contact point number from 0.5 to 1.0 mm lateral offset than the NT and AI groups (Fig. 7A). The contact point number of the BI group in the 200 µm virtual articulating paper increased with an increase in lateral offset until 2 mm and then decreased, which differs from the other three groups (Fig. 7B).

A significant difference ($p < 0.05$) was found in the contact point number of the BI group compared with the AI and TD groups using 100 µm virtual articulating paper at a 0.5 mm horizontal displacement. No significant differences were found between the other groups regarding the contact point numbers with horizontal displacements (*i.e.* 0.5, 1.0, 2.0, and 3.0 mm). The difference between all groups regarding the contact point area with 0.5-, 1.0-, 2.0, and 3.0 mm horizontal displacements was insignificant (Fig. 7C and 7D).

As illustrated in Fig. 8, the occlusion steepness continuously decreased for all groups as the lateral offset increased. The NT and AI groups had no significant differences, whereas significant differences were found between the BI and TD groups, which had significantly lower occlusal steepness than the NT and AI groups, indicating flatter occlusal surfaces in the BI and TD groups.

3.4. *Dynamic finite element analysis*

The stress distributions of the adhesive resin cement layer and abutment under physiological occlusal forces (300 N) are shown in Figs. 9–12. The corresponding numerical values of the stresses are listed in Table 4. Areas around the central fossa and contact points on the models were selected for measurement.

As shown in Table 4, stresses at the central fossa area were generally lower than those at the contact point area, except in the BI group. The TD group had the highest stress value in both measured areas. In the inner layers of the crown (*i.e.* the adhesive layer and dentine), the maximum principal stress and shear stress varied. The AI group had the highest maximum principal stress, followed by the NT, TD, and BI groups in dentine. In the adhesive layer, the TD group had the highest maximum principal stress, followed by the

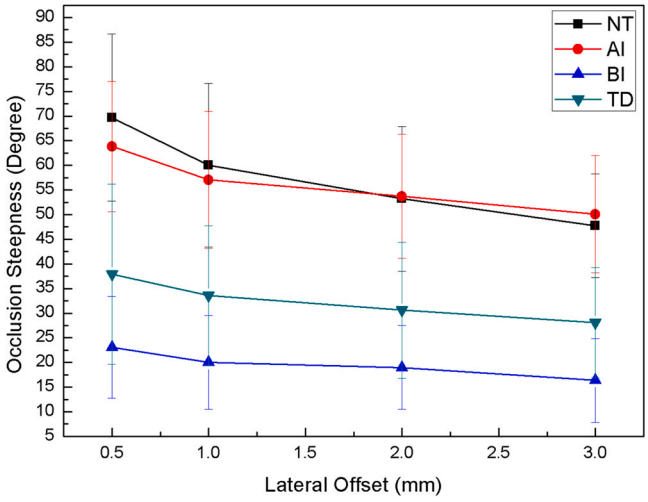

Fig. 8 – Trend of mean occlusion steepness when increasing the offset from 0.5 to 3 mm on the lateral occlusion.

AI, NT, and BI groups. An obvious distinction was found in the maximum shear stress for the TD group, which was 2.5–4 times lower than that of the other three groups.

As shown in Figs. 9–12, the maximum principal stress and maximum Tresca (shear) stress of the adhesive layer and dentine were observed in the shoulder area. In contrast, as expected, no stress concentrations were found in the occlusal directions of the adhesive layer and dentine in all cases, as the shoulder area should be the main load-bearing structure. Among all the cases analysed by FE, as shown in Fig. 12, the TD crown showed a high-stress concentration in both the dentine and adhesive layers compared to the other models.

The fatigue-life circles were estimated. As illustrated in Fig. 13, the AI group had the closest estimated fatigue lifetime compared with the NT group. The AI group achieved *ca.* 10e32 (10^{32}) cycle lifetime in the area near the contact area and *ca.* 10e35 (10^{35}) cycles in the central fossa area under 400 N loading, while the numbers in the NT group were determined to be *ca.* 10e38 (10^{38}) for both areas.

4. Discussion

AI-generated crowns by 3D-DCGAN revealed a higher degree of similarity with natural teeth (NT) morphology regarding cusp angle, MPD, MND, RMS, and fatigue biomechanics than the BI and TD groups. The proposed 3D-DCGAN learns from natural teeth, whereas BI and TD have different mechanisms. BI utilised a tooth library, and a technician made adjustments. Regarding TD, as there are no regulated standards for the design of occlusal surfaces, the position and dimensions of the design, such as groves and cusps, vary. Different technicians may have different preferences and ideas. Current designs mainly rely on crown's intra-oral 'try-in' to evaluate its quality. If patients found no discomfort or a 'high' bite, then this design is acceptable. However, the design aspects shown in this study can affect the biomechanical performance and thus exhibit different fatigue lifetimes (Fig. 13). The small differences in design played an essential role in the long-term success rate.

According to the heat map (Fig. 5), based on the 3D standard deviation results, the maximum positive/negative deviations frequently appeared at the groove or central fossa area in most cases. This may be due to the relatively lower accuracy of intraoral scanners in detecting Z-axis (depth) data. The precision of digital scanners is an essential factor in maintaining the accuracy of the dental crown design. Many

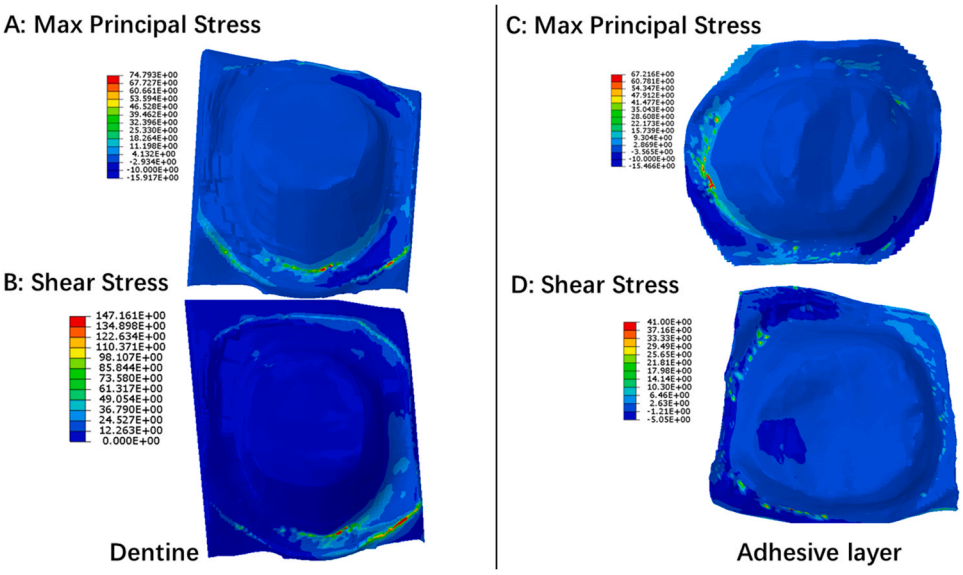

Fig. 9 – Max principal stress (A,C) and Tresca (Shear) stress (B,D) of tooth preparation (A,B) and adhesive cement layer (C,D) forthe NT group.

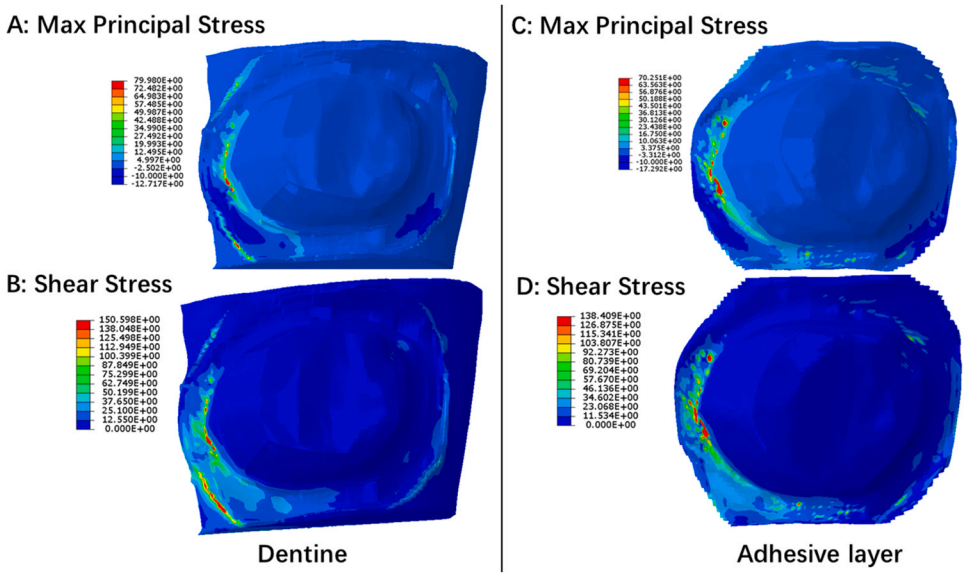

Fig. 10 – Max principal stress (A,C) and Tresca (Shear) stress (B,D) of tooth preparation (A,B) and adhesive cement layer (C,D) for the AI group.

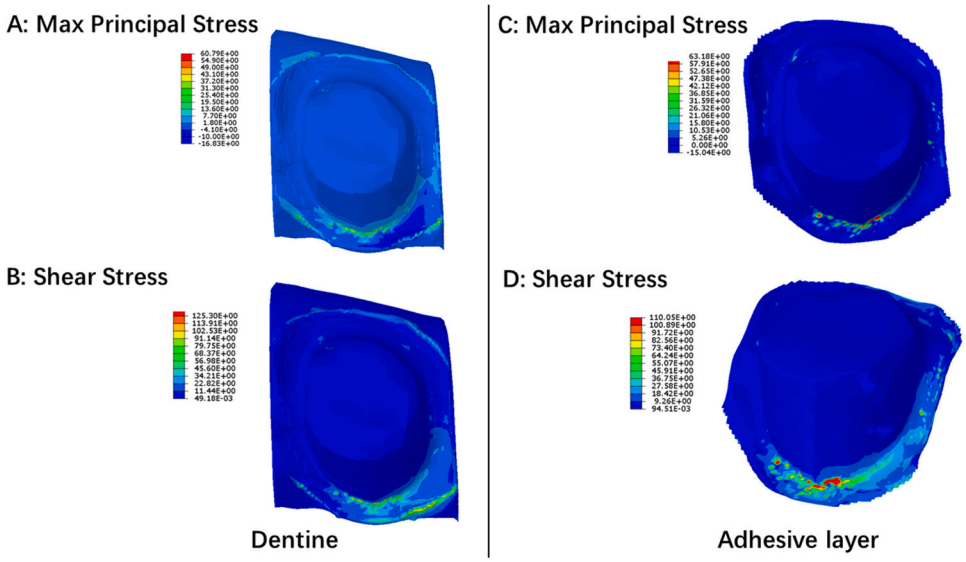

Fig. 11 – Max principal stress (A,C) and Tresca (Shear) stress (B,D) of tooth preparation (A,B) and adhesive cement layer (C,D) for the BI group.

studies have revealed that the accuracy of various intraoral and extraoral scanners must be improved, especially for full-arch scanning. A 50 µm accuracy level is sufficient for manufacturing [31]. Some studies have indicated that intraoral scanners have more errors in Z-axis (depth) scanning [32,33]. This might explain the maximum discrepancy in AI-generated crowns that often appeared around the groove or central fossa area, as they were usually the lowest areas on the occlusal surface.

Two different approaches were used in this study to measure the number and area of occlusal contact points. In Geomagic software, the measurement of occlusal contact was achieved by vertically shifting the crowns manually to be measured, followed by Boolean operation and maintaining the intersection part of the crown and the opposing dentition. While Meshlab software created a distance map between the crown and the opposing dentition, occlusal contact can be calculated by filtering the mesh vertices with distances less than

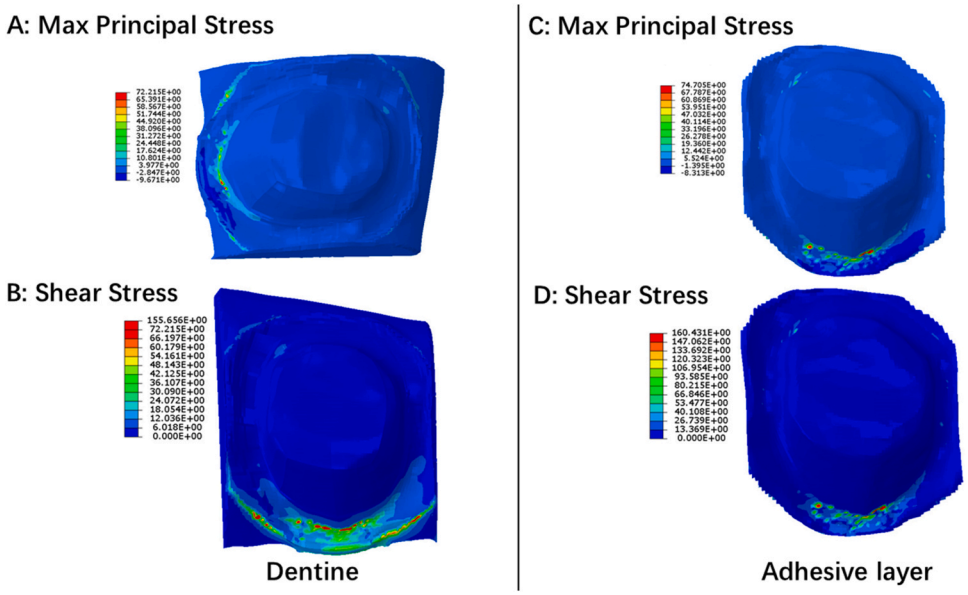

Fig. 12 – Max principal stress (A,C) and Tresca (Shear) stress (B,D) of tooth preparation (A,B) and adhesive cement layer (C,D) for the TD group.

200 µm. Several studies have used software for dental occlusion research [20,34–36]. However, none of these studies compared the uniformity of the two approaches. Although implemented by different approaches in measuring occlusal contacts, we found very high uniformity in the results measured by the two software programs. The deviation was calculated to be within 5 % of all the occlusal contacts measured in this study. Both software programs can be useful tools for measuring occlusal contact in dentistry.

Occlusion remains a long-standing challenge in prosthodontics. The occlusal evaluation cannot only be based on static occlusion. Dynamic occlusion is critical for the design of a good dental crown. To better simulate the trajectory of the tooth, lateral movement of the crowns at four horizontal excursive positions (0.5–3.0 mm) from the maximal intercuspation was adopted. The occlusal contact number and area decreased as the lateral movement increased in most cases, except in the BI group. This result was consistent with that of Ogawa et al. [37]. In this study, the steepness of the occlusal area was measured. From the viewpoint of anatomic features, the fossa area is steeper than the cuspal area [38], which is in accordance with our results.

In our study, the occlusal contact point number and area showed no significant differences among the four groups, as the data variation was quite significant with high SDs. This result identifies with a study from Watanabe-Kanno et al. [39]. The number and area of contact points depend on the individual's anatomy. In addition, the degrees of overjet and overbite are important factors that influence occlusal contact [40,41].

This study semi-quantitatively evaluated the biomechanical performance of an AI-generated 3D dental subject using an *in silico* fatigue developed by Homaei et al. [16], a validated dynamic non-linear FE model encompassing multi-layered teeth, materials (crown and resin cement), and design. This model closely matched the simulated fatigue lifetimes and experimental results for premolar crowns with different materials. Ideally, FEA estimates the fatigue properties based on the material type, stress distribution, Young's modulus, and Poisson's ratio, and it represents the condition that all parts of the model are homogeneous, isotropic, and linearly elastic. However, the material used in the experimental setup may have some nonhomogeneous structures, and the interfaces within the model may not have a constant elastic modulus or strength. The inconsistency between the

Table 4 – Stress distribution on crowns, maximum principal and shear stress on adhesive layer and dentine area with different designs subjected to physiological occlusal forces.

Groups	Stress Distribution on Crown		Max Stresses on Dentine		Max Stresses on Adhesive Layer	
	Central Fossa Area (MPa)	Around Contact Area (MPa)	Max. Principal Stress (MPa)	Max. Shear Stress (MPa)	Max. Principal Stress (MPa)	Max. Shear Stress (MPa)
NT	23.97	24.13	74.79	147.16	67.22	41.00
AI	26.73	28.48	79.98	150.60	70.25	138.41
BI	20.04	18.90	60.79	125.30	63.18	110.05
TD	40.72	54.18	72.22	155.66	74.71	160.43

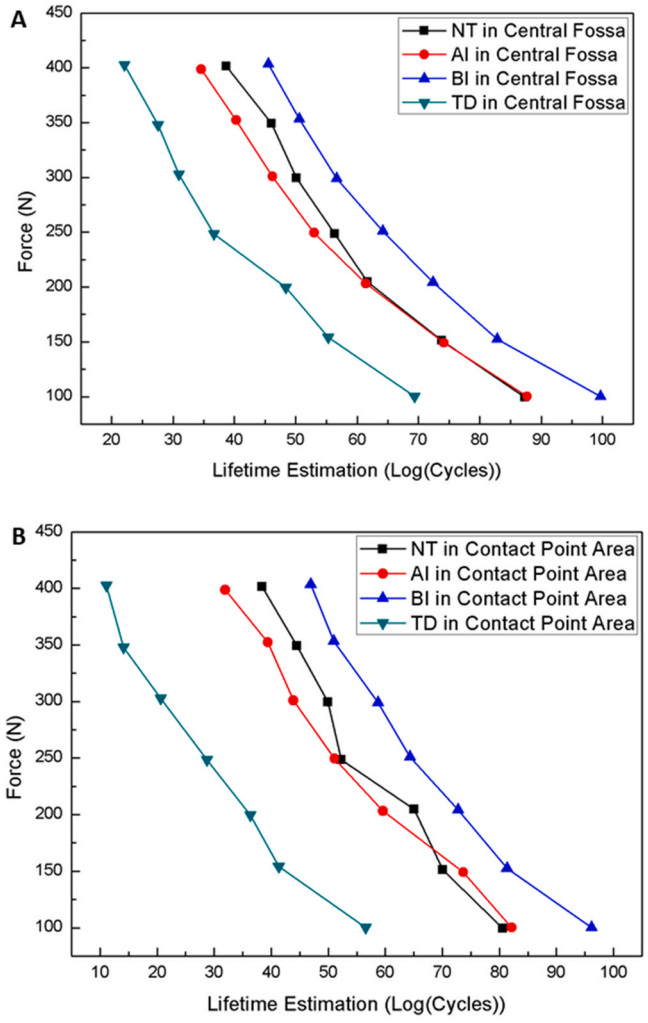

Fig. 13 – Force *vs.* lifetime estimation (in log scale) for the crown designs in (A) central fossa area and (B) contact point area.

theoretical simulation and experimental study causes higher fatigue lifetimes in the simulation than in the experimental results. Even so, the numbers still showed good correlations, at least in consistency.

In FEA, the amount of loading applied to the indenter was determined based on the average fatigue failure loads in an experimental study [42]. A previous study [43] formulated an S–N fatigue curve for LD dental ceramics. Using the fatigue properties of the LD material from the reported S-N curve and finding the stress value in the presented ceramic crowns, the number of cycles under loading can be calculated using the non-linear Basquin formula [26,27]. The present study considered different occlusal forces (100–400 N). The stress values were computed for each load. The Force vs. lifetime curve (F-N curve) was used to compare the lifetime of each crown design in an informative approach. This representation provides valuable information on the lifetimes of different crown designs and their relationships with exceeding loading. However, it should be noted that the estimated lifetime based on the FEA has some limitations. Owing to the complex geometry of dental crowns, various parameters, such as the degree of the polished surface and the possible microcracks, may affect the failure phenomena. For instance, monitoring the initiation of a microcrack can provide more insightful data on the lifetime of a ceramic crown than recording the maximum stress. Thus, the FE models in the present study can be improved using various advanced computational methods to estimate the lifetime [44–46].

5. Conclusion

We proposed a new artificial intelligence (AI) approach to design dental crowns based on a true 3D deep learning algorithm (3D-DCGAN) that showed the least discrepancy with natural teeth compared to BI and TD. Regarding occlusal contact point and area, 3D-DCGAN, BI, and TD have comparable occlusal relationships that match well with natural teeth. Regarding the fatigue properties of lithium disilicate crowns, dynamic FEA revealed no stress concentration for 3D-DCCAN-designed crowns, and the estimated lifetime was best matched with natural teeth.

CRediT authorship contribution statement

H. Ding: Contributed to design, data acquisition, analysis, and interpretation, drafted and critically revised the manuscript; Z. Cui and E. Maghami: Contributed to analysis and interpretation; Y. Chen: Contributed to data acquisition; W. Wang, J.P. Matinlinna and M.F. Burrow: Contributed to conception, critically revised the manuscript; E.H.N. Pow and Alex Fok: Contributed to grant acquisition and critically revised the manuscript. J.K.H. Tsoi: Contributed to grant acquisition, conception and design, data analysis and interpretation, drafted and critically revised the manuscript. All authors gave their final approval and agreed to be accountable for all aspects of the work.

Acknowledgements

This work is submitted in partial fulfilment of the requirements of the degree of PhD for the first author at the Faculty of Dentistry, The University of Hong Kong. Part of the data has been presented in the 35th Annual Scientific Meeting of the IADR-SEA Division, Hong Kong, along with support from IADR-SEA Research Category Award (Dental Materials and Biomaterials Category) in 2021. This research study is supported by General Research Fund from the Research Grants Council, Hong Kong (GRF 17120220), Health and Medical Research Fund from the Health Bureau, The Government of the Hong Kong SAR (HMRF 08193056), and Innovation and Technology Fund from Innovation and Technology Commission, The Government of the Hong Kong SAR (MHP/075/20).

REFERENCES

[1] Norvig P. Artificial intelligence: early ambitions. N Sci 2012. 216:ii-iii.

[2] Mehl A, Blanz V, Hickel R. Biogeneric tooth: a new mathematical representation for tooth morphology in lower first molars. Eur J Oral Sci 2005;113:333–40.
[3] Mehl A, Blanz V. New procedure for fully automatic occlusal surface reconstruction by means of a biogeneric tooth model. Int J Comput Dent 2005;8:13–25.
[4] Atlas A, Isleem W, Bergler M, Fraiman HP, Walter R, Lawson ND. Factors affecting the marginal Fit of CAD-CAM restorations and concepts to improve outcomes. Curr Oral Health Rep 2019;6:277–83.
[5] Chen Y, Lee JKY, Kwong G, Pow EHN, Tsoi JKH. Morphology and fracture behavior of lithium disilicate dental crowns designed by human and knowledge-based AI. J Mech Behav Biomed Mater 2022;131:105256.
[6] Hwang J-J, Jung Y-H, Cho B-H, Heo M-S. An overview of deep learning in the field of dentistry. Imaging Sci Dent 2019;49:1–7.
[7] Ding H, Wu J, Zhao W, Matinlinna JP, Burrow MF, Tsoi JK-H. Artificial intelligence in dentistry – a review. Front Dent Med 2023;4:1085251.
[8] Goodfellow I, Pouget-Abadie J, Mirza M, Xu B, Warde-Farley D, Ozair S, et al. Generative adversarial nets. Adv Neural Inf Process Syst 2014:27.
[9] Hwang J.-J., Azernikov S., Efros A.A., Yu S.X. Learning beyond human expertise with generative models for dental restorations. arXiv preprint arXiv:180400064. 2018.
[10] Yuan F, Dai N, Tian S, Zhang B, Sun Y, Yu Q, et al. Personalized design technique for the dental occlusal surface based on conditional generative adversarial networks. Int J Numer Method Biomed Eng 2020;36:e3321.
[11] Radford A., Metz L., Chintala S. Unsupervised representation learning with deep convolutional generative adversarial networks. arXiv preprint arXiv:151106434. 2015.
[12] Wu J., Zhang C., Xue T., Freeman W.T., Tenenbaum J.B. Learning a probabilistic latent space of object shapes via 3d generative-adversarial modeling. Proceedings of the 30th International Conference on Neural Information Processing Systems 2016. p. 82–90.
[13] Wiskott HA, Belser UC. A rationale for a simplified occlusal design in restorative dentistry: historical review and clinical guidelines. J Prosthet Dent 1995;73:169–83.
[14] Türp JC, Greene C, Strub J. Dental occlusion: a critical reflection on past, present and future concepts. J Oral Rehabil 2008;35:446–53.
[15] Maghami E, Homaei E, Farhangdoost K, Pow EHN, Matinlinna JP, Tsoi JK-H. Effect of preparation design for all-ceramic restoration on maxillary premolar: a 3D finite element study. J Prosthodont Res 2018;62:436–42.
[16] Homaei E, Jin X-Z, Pow EHN, Matinlinna JP, Tsoi JK-H, Farhangdoost K. Numerical fatigue analysis of premolars restored by CAD/CAM ceramic crowns. Dent Mater 2018;34:e149–57.
[17] Cignoni P., Callieri M., Corsini M., Dellepiane M., Ganovelli F., Ranzuglia G. Meshlab: an open-source mesh processing tool. Eurographics Italian Chapter Conference: Salerno, Italy; 2008. p. 129–36.
[18] Wan B, Shahmoradi M, Zhang Z, Shibata Y, Sarrafpour B, Swain M, et al. Modelling of stress distribution and fracture in dental occlusal fissures. Sci Rep 2019;9:4682.
[19] Abduo J, Bennamoun M, Tennant M, McGEACHIE J. Effect of prosthodontic planning on lateral occlusion scheme: a comparison between conventional and digital planning. J Appl Oral Sci 2015;23:196–205.
[20] Abduo J. Geometrical effects of conventional and digital prosthodontic planning wax-ups on lateral occlusal contact number, contact area, and steepness. J Oral Sci 2017;59:431–8.
[21] Grosland NM, Shivanna KH, Magnotta VA, Kallemeyn NA, DeVries NA, Tadepalli SC, et al. IA-FEMesh: an open-source, interactive, multiblock approach to anatomic finite element model development. Comput Methods Prog Biomed 2009;94:96–107.
[22] Dejak B, Młotkowski A, Langot C. Three-dimensional finite element analysis of molars with thin-walled prosthetic crowns made of various materials. Dent Mater 2012;28:433–41.
[23] Andreaus U, Colloca M, Iacoviello D. Coupling image processing and stress analysis for damage identification in a human premolar tooth. Comput Methods Prog Biomed 2011;103:61–73.
[24] Jiang W, Bo H, Yongchun G, LongXing N. Stress distribution in molars restored with inlays or onlays with or without endodontic treatment: a three-dimensional finite element analysis. J Prosthet Dent 2010;103:6–12.
[25] Dejak B, Młotkowski A. Three-dimensional finite element analysis of strength and adhesion of composite resin versus ceramic inlays in molars. J Prosthet Dent 2008;99:131–40.
[26] Mutluay MM, Yahyazadehfar M, Ryou H, Majd H, Do D, Arola D. Fatigue of the resin–dentin interface: a new approach for evaluating the durability of dentin bonds. Dent Mater 2013;29:437–49.
[27] Yahyazadehfar M, Mutluay MM, Majd H, Ryou H, Arola D. Fatigue of the resin–enamel bonded interface and the mechanisms of failure. J Mech Behav Biomed Mater 2013;21:121–32.
[28] Ausiello P, Franciosa P, Martorelli M, Watts DC. Numerical fatigue 3D-FE modeling of indirect composite-restored posterior teeth. Dent Mater 2011;27:423–30.
[29] Nalla RK, Kinney JH, Marshall SJ, Ritchie RO. On the in vitro fatigue behavior of human dentin: effect of mean stress. J Dent Res 2004;83:211–5.
[30] Ye Y, Di P, Jia S, Lin Y. Occlusal force and its distribution in the position of maximum intercuspation in individual normal occlusion: a cross-sectional study. Zhong Hua Kou Qiang Yi Xue Za Zhi = Chin J Stomatol 2015;50:536–9.
[31] Rudolph H, Luthardt RG, Walter MH. Computer-aided analysis of the influence of digitizing and surfacing on the accuracy in dental CAD/CAM technology. Comput Biol Med 2007;37:579–87.
[32] Amornvit P, Rokaya D, Sanohkan S. Comparison of accuracy of current ten intraoral scanners. Biomed Res Int 2021;2021:2673040.
[33] Nagy Z, Simon B, Mennito A, Evans Z, Renne W, Vág J. Comparing the trueness of seven intraoral scanners and a physical impression on dentate human maxilla by a novel method. BMC Oral Health 2020;20:1–10.
[34] Buschang PH, Ross M, Shaw SG, Crosby D, Campbell PM. Predicted and actual end-of-treatment occlusion produced with aligner therapy. Angle Orthod 2015;85:723–7.
[35] Xiao N, Sun Y, Zhao Y, Wang Y. Preliminary study on three digital analysis methods for analyzing the distribution and area of occlusal contacts. J Peking Univ, Health Sci 2020;52:144–51.
[36] Solaberrieta E, Otegi JR, Goicoechea N, Brizuela A, Pradies G. Comparison of a conventional and virtual occlusal record. J Prosthet Dent 2015;114:92–7.
[37] Ogawa T, Ogimoto T, Koyano K. Pattern of occlusal contacts in lateral positions: canine protection and group function validity in classifying guidance patterns. J Prosthet Dent 1998;80:67–74.
[38] Wang M, Mehta N. A possible biomechanical role of occlusal cusp–fossa contact relationships. J Oral Rehabil 2013;40:69–79.
[39] Watanabe-Kanno GA, Abrão J. Study of the number of occlusal contacts in maximum intercuspation before orthodontic treatment in subjects with Angle Class I and

Class II Division 1 malocclusion. Dent Press J Orthod 2012;17:138–47.
[40] Magalhães IB, Pereira LJ, Marques LS, Gameiro GH. The influence of malocclusion on masticatory performance: a systematic review. Angle Orthod 2010;80:981–7.
[41] Al-Rayes NZ, Hajeer MY. Evaluation of occlusal contacts among different groups of malocclusion using 3D digital models. J Conte Dent Pr 2014;15:46–55.
[42] Homaei E, Farhangdoost K, Pow EHN, Matinlinna JP, Akbari M, Tsoi JK-H. Fatigue resistance of monolithic CAD/CAM ceramic crowns on human premolars. Ceram Int 2016;42:15709–17.
[43] Homaei E, Farhangdoost K, Tsoi JKH, Matinlinna JP, Pow EHN. Static and fatigue mechanical behavior of three dental CAD/CAM ceramics. J Mech Behav Biomed Mater 2016;59:304–13.
[44] Carrara P, Ambati M, Alessi R, De, Lorenzis L. A framework to model the fatigue behavior of brittle materials based on a variational phase-field approach. Comput Methods Appl Mech Eng 2020;361:112731.
[45] Maghami E, Pejman R, Najafi AR. Fracture micromechanics of human dentin: a microscale numerical model. J Mech Behav Biomed Mater 2021;114:104171.
[46] Desmorat R, Ragueneau F, Pham H. Continuum damage mechanics for hysteresis and fatigue of quasi-brittle materials and structures. Int J Numer Anal Methods Geomech 2007;31:307–29.